Geomechanics and Engineering, *Vol. 25, No. 4 (2021) 303-315*
DOI: https://doi.org/10.12989/gae.2021.25.4.303

A similarity solution for undrained expansion of a cylindrical cavity in K_0-consolidated anisotropic soils

You Wang[2a], Lin Lin*[1] and Jingpei Li[2b]

[1]*School of Highway, Chang'an University, Xi'an 710064, China*
[2]*Department of Civil Engineering, Tongji University, Shanghai 200092, China*

(Received August 24, 2020, Revised April 3, 2021, Accepted May 11, 2021)

Abstract. A rigorous and generic similarity solution is developed for assessment of the undrained expansion responses of a cylindrical cavity expansion in K_0-consolidated anisotropic soils. A K_0-consolidated anisotropic modified Cam-clay (K_0-AMCC) model that can represent the initial stress anisotropy and the effects of stress-induced anisotropy is used to model the soil behaviors during cavity expansion. All the seven basic unknowns, the three stress components, the pore water pressure, the particle velocity, the specific volume and the hardening parameter, are reduced to the functions of a dimensionless radial coordinate and are taken as coupled variables to formulate the problem. The governing equations are formulated by making use of the equilibrium equation, the constitutive equation, the consistency condition, the continuity condition and the undrained condition, which are then solved as an initial value problem. The proposed rigorous similarity solution is compared with some well-documented rigorous solutions to validate the solution and to highlight the special expansion responses in anisotropic soils. The results reveal that the present solution can yield more predictions for cavity expansion problems in soils with initial anisotropic stresses.

Keywords: similarity solution; cavity expansion; undrained condition; anisotropy

1. Introduction

The cavity expansion, which is a fundamental but complicated problem, has been widely utilized to predict the capacity of driven piles (Wroth and Windle 1975, Houlsby and Withers 1988, Cudmani and Osinov 2001, Marshall 2012, Gao *et al.* 2021) and to interpret the pressuremeter tests, the cone penetration tests and the grouting process (Cudmani and Osinov 2001, Salgado *et al.* 1997, Chang *et al.* 2001, Zou and Zuo 2017, Moug *et al.* 2019, Wang *et al.* 2020, Peng *et al.* 2021). In the past decades, many advanced constitutive models have been applied to capturing soil or rock behaviors in the cavity expansion theory (Ladanyi 1963, Carter *et al.* 1986, Collins and Stimpson 1994, Chen and Abousleiman 2012, Silvestri and Abou-Samra 2012, Matsuoka and Sun 2014, Li *et al.* 2017, Zou and Xia 2017, Johnsen *et al.* 2018, Zhou *et al.* 2016, 2017, 2018, dos Santos *et al.* 2019, Zou *et al.* 2019, Yang *et al.* 2020, Mo *et al.* 2020a, b, 2021, Li *et al.* 2021, Yang *et al.* 2021a, b)

Due to the complex elastoplastic properties of soils, it is theoretically hard to get rigorous analytical or semi-analytical solution for cavity expansion problems. Hence, many semi-analytical and numerical solutions have been proposed over the past few decades. Ladanyi (1963) investigated cavity expansion responses employing stress-strain curves determined from the triaxial tests. It is obvious that the accuracy of their solution greatly depends on the stress-strain relation from the tests. Randolph *et al.* (1979) investigated the installation effects of a driven pile by modeling the installation process as undrained expansion of a cylindrical cavity. In their solution, a simplified Cam-clay model was employed to capture soil behaviors during the process of cavity expansion. Carter *et al.* (1986) developed a rigorous closed-form solution for cavity expansion in an idealized cohesive-frictional soil and proposed an explicit expression for the expansion-pressure relation. Collins and Stimpson (1994) presented a unified similarity solution to cavity expansion problems in isotropic material. Cao *et al.* (2001) developed a semi-analytical solution and an approximate closed-form solution to undrained cavity expansion in MCC soils by simplifying the deviator stress. Russell and Khalili (2002) proposed an analytical solution to drained cavity expansion in sands by adopting the similarity technique and a modified state parameter model. The solution considered the effect of particle crushing during the cavity expansion process (e.g. cone penetration test) in sands. Based on the rigorous definitions of the two stress invariants, Chen and Abousleiman (2012) presented a novel, rigorous and standard semi-analytical framework for undrained expansion of a cylindrical cavity in critical state soils. However, the effects of soil anisotropy cannot be appropriately modeled by the MCC model based isotropic solution. To investigate the effects of the soil anisotropy on the cavity expansion responses, Li *et al.* (2016) and Li *et al.*

*Corresponding author, Ph.D.
E-mail: 1310230@tongji.edu.cn
[a]Ph.D.
E-mail: youwangtony@163.com
[b]Professor
E-mail: lijp2773@tongji.edu.cn

http://www.techno-press.org/?journal=gae&subpage=7
ISSN: 2005-307X (Print), 2092-6219 (Online)

Table 1 Summary of recent publications about cavity expansion theories

Literature	Main contents of research	Type of approach
Ladanyi (1963)	Obtaining cavity expansion responses with stress-strain curves from triaxial tests	Experimental
Randolph *et al.* (1979)	Investigating pile installation effects using cavity expansion theories	Analytical
Carter *et al.* (1986)	Developing cavity expansion solutions in idealized cohesive-frictional soils	Analytical
Collins and Stimpson (1994)	Proposing a similarity solution to cavity expansion problems	Semi-analytical
Li *et al.* (2016) and Li *et al.* (2017)	Developing undrained and drained elastoplastic cavity expansion solutions based on K_0-AMCC	Semi-analytical
Sivasithamparam and Castro (2018)	Investigating undrained cylindrical cavity expansion in fabric anisotropic soils	Semi-analytical
Li and Zou (2019)	Developing undrained cavity expansion solutions in anisotropic soils based on SMP criterion	Analytical

(2017) derived elastoplastic solutions to cavity expansion under both undrained and drained conditions based on a K_0 consolidated modified Cam-clay (K_0-AMCC) model. Vrakas (2016) presented a generic solution, which can be applied for any two-invariant constitutive models, for undrained expansion of a cylindrical cavity in critical state soils. Based on the advanced S-CLAY1 soil model (2003), Sivasithamparam and Castro (2018) developed a semi-analytical solution following the framework of Chen and Abousleiman (2012), which could properly consider the initial anisotropy and the fabric anisotropy changes during cavity expansion, for undrained expansion of cylindrical cavity in fabric anisotropic soils. Nearly at the same time, a rigorous semi-analytical solution was developed by Chen and Liu (2018) for cylindrical cavity undrained expansion in anisotropic critical state soils based on the well-established anisotropic critical state model of Dafalias (1986) to explore the effects of initial stress anisotropy and the rotation hardening of the natural soil on the expansion responses. By implementing the Spatially Mobilized Plane (SMP) criterion, Chen *et al.* (2019) proposed analytical solutions that consider the three-dimensional strength of the soil to cylindrical cavity expansion problems in anisotropic soils. Li and Zou (2019) also presented a closed-form solution to undrained cavity expansion in anisotropic soils, integrating the SMP criterion into the analysis as well. Some significant publications regarding cavity expansion theories have been listed in Table 1 in order to enable a clear view of recent contributions to this field. It can be discerned that although a variety of solutions have been developed for cavity expansion problems recently, most of these solutions are based on the isotropic and elastic-perfectly plastic assumptions. There is nearly a dearth of similarity solution that considers the effects of the stress anisotropy for cavity expansion problems. Since a generic similarity solution is not available at present for cavity expansion in anisotropic soils, it is of great significance to develop a similarity solution for cavity expansion in anisotropic soils.

This paper presents a similarity solution for undrained expansion of a cylindrical cavity in K_0-AMCC soils. The initial stress anisotropy and the evolution of the stress anisotropy are modeled by the K_0-AMCC model of Sekiguchi and Ohta (1977). According to the analytical framework of similarity solution (1994), the basic unknowns, including the three stress components, the particle velocity, the pore water pressure, the specific volume and the hardening parameter, are reduced to the functions of a dimensionless radial coordinate. The advantage of the present solution over the similarity solution of Collins and Stimpson (1994) lies in that the current solution takes the rigorous definition of the deviatoric stress and properly considers the anisotropy of soils. Furthermore, the volume conservation condition is used to determine the real radial coordinate rather than the dimensionless coordinate in this study. Another noteworthy point is that the proposed solution is developed within the framework of similarity solution technique and considers all the seven basic unknown variables involved in the problem, while the solution of Li *et al.* (2016) was derived in terms of Lagrangian description and only considered *three* basic unknown variables. Hence the analytical framework of the present solution is different from the solution of Li *et al.* (2016) and is more generic, although the two solutions focus on the same topic. The proposed similarity solution is validated by comparing the expansion-pressure curves, the development of excess pore pressure at the cavity wall and the distributions of stress components around the cavity with those obtained from the rigorous semi-analytical solution of Li *et al.* (2016). The current similarity solution provides an alternative rigorous solution technique for undrained cavity expansion problems, which are expected to serve as a benchmark to validate other rigorous solutions or numerical simulations for cavity expansion problems with critical constitutive soil models.

2. Anisotropic critical soil model

Roscoe and Burland (1968) first presented the classical modified Cam-clay (MCC) model on the basis of the critical state concept, which could well represent the elastoplastic behavior of the isotropic clays. Nevertheless, the MCC model cannot represent the anisotropic properties of K_0-consolidated natural soil during cavity expansion. Therefore, a K_0-AMCC model of Sekiguchi and Ohta (1977) that properly considers the anisotropic behaviors of the natural soils was adopted to derive the present solution.

As seen in Fig. 1, The yield surface of the K_0-AMCC model is a rotated and distorted ellipse in the $p'-q$ plane, and the degree of declination reflects the extent of anisotropy of the soil. The yield function of the model can be written as

$$f = 1 + (\frac{\eta^*}{M^*})^2 - \frac{p'_c}{p'} = 0 \tag{1}$$

where p'_c is the hardening parameter of the K_0-MCC model; p' represents the mean effective stress; η^* is the relative stress ratio; M^* is the relative stress ratio at the critical state. The expressions of η^* and M^* defined as

$$\eta^* = \sqrt{\frac{3}{2}(\eta_{ij} - \eta_{ij0})(\eta_{ij} - \eta_{ij0})} \tag{2}$$

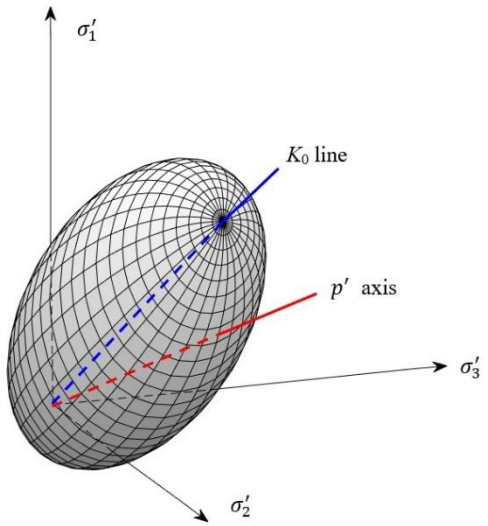

Fig. 1 Yield surface in principle stress space

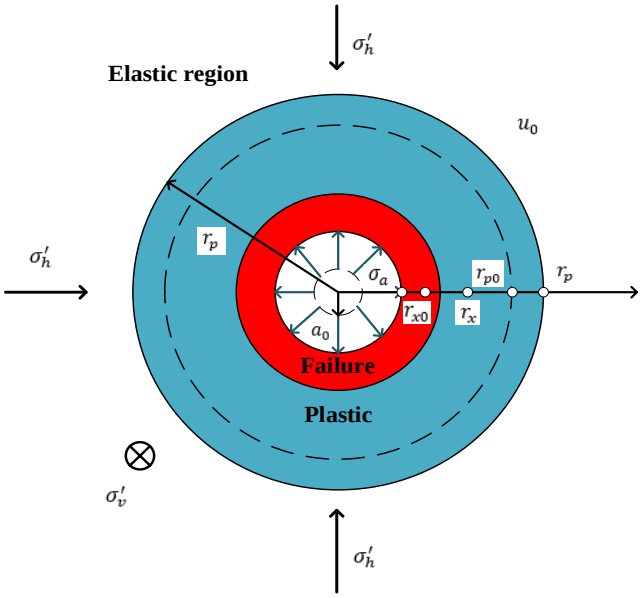

Fig. 2 Schematic of cylindrical cavity expansion in anisotropic clay

$$M^* = \sqrt{M^2 - \eta_0^2} \tag{3}$$

where

$$\eta_{ij} = \frac{\sigma_{ij}' - p'\delta_{ij}}{p'} \tag{4}$$

$$\eta_{ij0} = \frac{\sigma_{ij0}' - p_0'\delta_{ij}}{p_0'} \tag{5}$$

$$\eta_0 = \left|\frac{3(1-K_0)}{2K_0+1}\right| \tag{6}$$

$$M = \frac{6\sin\varphi'}{3-\sin\varphi'} \tag{7}$$

where φ' denotes the internal friction angle of the soil; p_0' denotes the initial mean effective stress; σ_{ij}' represent the tensor of the effective stress; K_0 is the earth pressure coefficient at rest, and δ_{ij} is Kronecker's delta.

3. Definitions and basic assumptions

Fig. 2 schematically shows the top view of a cylindrical cavity expands from the initial radius of a_0 to current radius a in the K_0-consolidated anisotropic soil. During the expansion process, the internal expansion pressure increases from the in-situ value, σ_h to current internal pressure σ_a. If the stress exceeds the yield stress of the soil, the soil at the cavity wall will yield first. As a result, a plastic zone will be developed around the cavity. During the expansion process, a soil particle which initially locates at r_{x0} moves radially outwards to a new position r_x. Correspondingly, the soil particle occupied at the elastic-plastic boundary will move from the initial position, r_{p0} to the current radial position, r_p.

The underlying assumptions made in development of the present solution are as follows

(a) Following the definition of soil mechanics, the compressive stress is defined as positive stress.

(b) The soil is regarded as a homogeneous material, while the anisotropy is referred to as the initial stress anisotropy, i.e., the initial horizontal effective stress σ_{h0}' is not equal to the initial vertical effective stress σ_{v0}'.

(c) The volume of the saturated anisotropic clay is uncompressible during the undrained expansion process.

(d) The small deformation theory and Hook's law are used to model the elastic deformation behavior of the soil, while the logarithmic strain and the K_0-AMCC model are employed to model the elastoplastic behavior of the soil after yielding.

(e) It is assumed that the axial strain remains zero during the cavity expansion, i.e., the cylindrical cavity expands under plain strain condition.

Seven basic unknowns, the effective stress components σ_r', σ_θ',, and σ_z', the hardening parameter, p_c', the pore water pressure u, the particle velocity ω and the specific volume υ are involved in the cylindrical cavity expansion problem. Although the problem can be essentially formulated by the three effective stress components under the undrained condition, all the seven parameters are taken as the coupled variables and determined from the coupled governing equations in this study to make the solution more generic. In order to get the similarity solution, the state variables should be firstly non-dimensionalized according to the framework of similarity solution technique (Collins and Stimpson, 1994). Since the specific volume υ is already a dimensionless variable, only the other six unknown state variables need to be non-dimensionalized by following equations

$$\bar{\omega} = \frac{\omega}{w},\ \bar{\sigma}_r' = \frac{\sigma_r'}{p_1'},\ \bar{\sigma}_\theta' = \frac{\sigma_\theta'}{p_1'},\ \bar{\sigma}_z' = \frac{\sigma_z'}{p_1'},\ \bar{p}_c' = \frac{p_c'}{p_1'},\ \bar{u} = \frac{u}{p_1'} \tag{8}$$

where ω is the radial expansion speed of an arbitrary soil

particle, and W is expansion speed of the soil particle at the elastic-plastic boundary; p_1' represents the reference stress used to normalize the stress components, which is taken as the initial mean effective stress p_0' in this study. As indicated by Collins and Stimpson (1994), the particle velocity and the unknown state variables and can be regarded as the functions of a non-dimensionalized radial coordinate η that is defined as

$$\eta = \frac{r}{r_p} \tag{9}$$

where r_p denotes the radius of the plastic region.

For a given soil particle, the time and the space derivatives are first defined to derive the solution for the cylindrical cavity expansion problem, which gives

$$\tilde{(\ )} = \breve{(\ )} + \omega \frac{\partial(\ )}{\partial r} \tag{10}$$

where $\tilde{(\ )}$ represents the derivative pertaining to the time, and $\breve{(\ )}$ denotes the derivative with respect to the space.

From the definition of the non-dimensionalized radial coordinate η, the following transformation can be obtained

$$\frac{\partial(\ )}{\partial r} = \frac{1}{r_p}\frac{\partial(\ )}{\partial \eta} \tag{11}$$

The derivative with regard to the local time can be expressed as

$$\breve{(\ )} = \frac{d(\ )}{d\eta}\frac{d\eta}{dt} = -\frac{W\eta}{r_p}\frac{d(\ )}{d\eta} \tag{12}$$

From Eqs. (10), (11) and (12), the time and the space derivative can be further expressed as follows

$$\tilde{(\ )} = \frac{W(\bar{\omega}-\eta)}{r_p}\frac{d(\ )}{d\eta} = \frac{W\beta}{r_p}\frac{d(\ )}{d\eta} \tag{13}$$

where $\beta = \bar{\omega} - \eta$.

4. Formulation of governing equations

4.1 Equilibrium equation

The equilibrium equation for the cylindrical cavity expansion problem can be expressed in the coordinate system as follows

$$\frac{d\sigma_r'}{dr} + \frac{du}{dr} + \frac{\sigma_r' - \sigma_\theta'}{r} = 0 \tag{14}$$

Applying Eq. (13) to (14), the dimensionless equilibrium equation can be given as

$$\frac{d\bar{\sigma}_r'}{d\eta} + \frac{d\bar{u}}{d\eta} + \frac{\bar{\sigma}_r' - \bar{\sigma}_\theta'}{\eta} = 0 \tag{15}$$

4.2 Constitutive equation

For the soil in the elastic state, the elastic strain increment can be determined by the stress increment based on Hooke's law as follows

$$\tilde{\varepsilon}_{ij}^e = \frac{1+\nu'}{E}\tilde{\sigma}_{ij}' - \frac{\nu'}{E}d\tilde{\sigma}_{mm}'\delta_{ij} \tag{16}$$

where E is the elastic modulus; ν' denotes the effective Poisson's ratio.

When the soil reaches plastic state, the total strain rate $\tilde{\varepsilon}_{ij}$ of the soil can be decomposed into the elastic part $\tilde{\varepsilon}_{ij}^e$ and the plastic part $\tilde{\varepsilon}_{ij}^p$. The elastic component can be determined by Eq. (16), while the plastic part should be calculated based on the *K₀-AMCC* model and the plasticity theory. The associated flow rule gives

$$\tilde{\varepsilon}_{ij}^p = \Lambda\frac{\partial f}{\partial \sigma_{ij}'} \tag{17}$$

where Λ is a plastic multiplier, which will be given as

$$\Lambda = -\frac{\frac{\partial f}{\partial \eta^*}\tilde{\eta}^* + \frac{\partial f}{\partial p'}\tilde{p}'}{\frac{\upsilon_0}{\lambda-\kappa}\frac{\partial f}{\partial p_c'}p_c'\left(\frac{\partial f}{\partial \sigma_r'} + \frac{\partial f}{\partial \sigma_\theta'} + \frac{\partial f}{\partial \sigma_z'}\right)} \tag{18}$$

where λ represents the slope of the isotropic compression line, κ is the slope of the swelling line, υ_0 is the initial value of the specific volume ratio. The detailed expressions of $\partial f/\partial \eta^*$, $\partial f/\partial p'$, $\partial f/\partial p_c'$ are given as

$$\frac{\partial f}{\partial \eta^*} = \frac{2\eta^*}{M^{*2}} \tag{19}$$

$$\frac{\partial f}{\partial p'} = \frac{p_c'}{p'^2} \tag{20}$$

$$\frac{\partial f}{\partial p_c'} = -\frac{1}{p'} \tag{21}$$

$$\tilde{\eta}^* = \frac{1}{2\eta^* p'}\left[3\left(\eta_{ij} - \eta_{ij0}\right) + \eta_{mn}(\eta_{mn} - \eta_{mn0})\delta_{ij}\right]\tilde{\sigma}_{ij}' \tag{22}$$

$$\tilde{p}' = \frac{\delta_{ij}}{3}\tilde{\sigma}_{ij}' \tag{23}$$

$$\frac{\partial f}{\partial \sigma_i'} = \frac{M^{*2}+\eta^{*2}}{3p'M^{*2}} + \frac{1}{p'M^{*2}}\left[3\left(\eta_{ij} - \eta_{ij0}\right) + \eta_{mn}(\eta_{mn} - \eta_{mn0})\right] \quad (i = r, \theta, z) \tag{24}$$

Substitution of Eq. (18) into Eq. (17), the rates of plastic strain can be further written as

$$\tilde{\varepsilon}_r^p = \frac{\lambda-\kappa}{1+e}\frac{M^{*2}+\eta^{*2}}{p'(M^2-\eta^2)}\left[\frac{1}{3} + \frac{3(\eta_r - \eta_{r0}) - \eta_{mn}(\eta_{mn} - \eta_{mn0})}{M^{*2}+\eta^{*2}}\right]\left[\frac{\delta_{ij}d\sigma_{ij}'}{3} + \frac{\left[3(\eta_r - \eta_{r0}) - \eta_{mn}(\eta_{mn} - \eta_{mn0})\delta_{ij}\right]\tilde{\sigma}_{ij}'}{M^{*2}+\eta^{*2}}\right] \tag{25}$$

$$\tilde{\varepsilon}_\theta^p = \frac{\lambda-\kappa}{1+e}\frac{M^{*2}+\eta^{*2}}{p'(M^2-\eta^2)}\left[\frac{1}{3} + \frac{3(\eta_\theta - \eta_{\theta0}) - \eta_{mn}(\eta_{mn} - \eta_{mn0})}{M^{*2}+\eta^{*2}}\right]\left[\frac{\delta_{ij}d\sigma_{ij}'}{3} + \frac{\left[3(\eta_r - \eta_{r0}) - \eta_{mn}(\eta_{mn} - \eta_{mn0})\delta_{ij}\right]\tilde{\sigma}_{ij}'}{M^{*2}+\eta^{*2}}\right] \tag{26}$$

$$\tilde{\varepsilon}_z^p = \frac{\lambda-\kappa}{1+e}\frac{M^{*2}+\eta^{*2}}{p'(M^2-\eta^2)}\left[\frac{1}{3}+\frac{3(\eta_z-\eta_{z0})-\eta_{mn}(\eta_{mn}-\eta_{mn0})}{M^{*2}+\eta^{*2}}\right]\left[\frac{\delta_{ij}d\sigma'_{ij}}{3}+\frac{[3(\eta_r-\eta_{r0})-\eta_{mn}(\eta_{mn}-\eta_{mn0})\delta_{ij}]\tilde{\sigma}'_{ij}}{M^{*2}+\eta^{*2}}\right] \quad (27)$$

where e represents the void ratio.

As stated previously, the large strain theory, i.e., logarithmic strain, is used to represent the strain-displacement relation. The logarithmic strains can be expressed in terms of the rate form as

$$\tilde{\varepsilon}_r = -\frac{\partial w}{\partial r};\ \ \tilde{\varepsilon}_\theta = -\frac{w}{r};\ \ \tilde{\varepsilon}_z = 0 \quad (28)$$

Combining Eqs. (16), (25)-(28), the constitutive law in rate form for the cylindrical cavity expansion problem can be given as

$$A_r\tilde{\sigma}'_r + A_\theta\tilde{\sigma}'_\theta + A_z\tilde{\sigma}'_z = -\frac{\partial w}{\partial r} \quad (29)$$

$$B_r\tilde{\sigma}'_r + B_\theta\tilde{\sigma}'_\theta + B_z\tilde{\sigma}'_z = -\frac{w}{r} \quad (30)$$

$$C_r\tilde{\sigma}'_r + C_\theta\tilde{\sigma}'_\theta + C_z\tilde{\sigma}'_z = 0 \quad (31)$$

where

$$A_r = aa_r^2 + \frac{1}{E}; A_\theta = aa_ra_\theta - \frac{\nu'}{E}; A_z = aa_ra_z - \frac{\nu'}{E} \quad (32)$$

$$B_r = aa_ra_\theta - \frac{\nu'}{E}; B_\theta = aa_\theta^2 + \frac{1}{E}; B_z = aa_\theta a_z - \frac{\nu'}{E} \quad (33)$$

$$C_r = aa_ra_z - \frac{\nu'}{E}; C_\theta = aa_\theta a_z - \frac{\nu'}{E}; C_z = aa_z^2 + \frac{1}{E} \quad (34)$$

$$a = \frac{\lambda-\kappa}{1+e}\frac{M^{*2}+\eta^{*2}}{p'(M^2-\eta^2)} \quad (35)$$

$$a_i = \frac{1}{3} + \frac{3(\eta_i-\eta_{i0})-\eta_{mn}(\eta_{mn}-\eta_{mn0})}{M^{*2}+\eta^{*2}} \quad (i = r,\theta,z) \quad (36)$$

Applying Eq. (13) to (29)-(31), the constitutive equation can be finally written in the dimensionless form as

$$\beta\bar{A}_r\frac{d\bar{\sigma}'_r}{d\eta} + \beta\bar{A}_\theta\frac{d\bar{\sigma}'_\theta}{d\eta} + \beta\bar{A}_z\frac{d\bar{\sigma}'_z}{d\eta} = -\frac{\partial\bar{\omega}}{\partial\eta} \quad (37)$$

$$\beta\bar{B}_r\frac{d\bar{\sigma}'_r}{d\eta} + \beta\bar{B}_\theta\frac{d\bar{\sigma}'_\theta}{d\eta} + \beta\bar{B}_z\frac{d\bar{\sigma}'_z}{d\eta} = -\frac{\bar{\omega}}{\eta} \quad (38)$$

$$\beta\bar{C}_r\frac{d\bar{\sigma}'_r}{d\eta} + \beta\bar{C}_\theta\frac{d\bar{\sigma}'_\theta}{d\eta} + \beta\bar{C}_z\frac{d\bar{\sigma}'_z}{d\eta} = 0 \quad (39)$$

where $\bar{A}_i$, $\bar{B}_i$ and $\bar{C}_i$ (i=r, θ, z) represent the normalized coefficients.

4.3 Plastic consistency equation

Following the plasticity theory, the plastic consistency condition of K_0-AMCC model can written as

$$\frac{\partial f}{\partial\sigma'_r}\tilde{\sigma}'_r + \frac{\partial f}{\partial\sigma'_\theta}\tilde{\sigma}'_\theta + \frac{\partial f}{\partial\sigma'_z}\tilde{\sigma}'_z + \frac{\partial f}{\partial p'_c}\tilde{p}'_c = 0 \quad (40)$$

Applying the differential chain rule to Eq. (40) gives

$$\left(\frac{\partial f}{\partial p'}\frac{\partial p'}{\partial\sigma'_r} + \frac{\partial f}{\partial\eta^*}\frac{\partial\eta^*}{\partial\sigma'_r}\right)\tilde{\sigma}'_r + \left(\frac{\partial f}{\partial p'}\frac{\partial p'}{\partial\sigma'_\theta} + \frac{\partial f}{\partial\eta^*}\frac{\partial\eta^*}{\partial\sigma'_\theta}\right)\tilde{\sigma}'_\theta + \left(\frac{\partial f}{\partial p'}\frac{\partial p'}{\partial\sigma'_z} + \frac{\partial f}{\partial\eta^*}\frac{\partial\eta^*}{\partial\sigma'_z}\right)\tilde{\sigma}'_z + \frac{\partial f}{\partial p'_c}\tilde{p}'_c = 0 \quad (41)$$

where

$$\frac{\partial\eta^*}{\partial\sigma'_i} = \frac{1}{2\eta^* p'}[3(\eta_r-\eta_{r0}) - \eta_{mn}(\eta_{mn}-\eta_{mn0})] \qquad i = r,\theta,z \quad (42)$$

$$\frac{\partial p'}{\partial\sigma'_i} = \frac{1}{3} \qquad i = r,\theta,z \quad (43)$$

Substitution of Eqs. (19), (20), (21), (42) and (43) into Eq. (41), the plastic consistency condition can be further expressed in the dimensionless form as

$$D_r\tilde{\sigma}'_r + D_\theta\tilde{\sigma}'_\theta + D_z\tilde{\sigma}'_z - \frac{1}{p'}\tilde{p}'_c = 0 \quad (44)$$

where

$$D_i = \frac{1}{3}\frac{p'_c}{p'^2} + \frac{1}{p'M^{*2}}[3(\eta_i-\eta_{i0}) - \eta_{mn}(\eta_{mn}-\eta_{mn0})] \qquad i = r,\theta,z \quad (45)$$

4.4 Continuity condition

For cylindrical cavity expansion problem, the rate of the total volumetric strain consists of the rates of the radial strain, tangential strain and the axial strain. Hence, the continuity condition can be given as

$$\tilde{\varepsilon}_v = \tilde{\varepsilon}_r + \tilde{\varepsilon}_\theta + \tilde{\varepsilon}_z \quad (46)$$

Substituting Eqs. (28) into Eq. (46) and applying Eq. (13), the dimensionless continuity equation for the problem considered can be obtained as

$$\beta\frac{d\upsilon}{d\eta} = \upsilon\frac{d\bar{\omega}}{d\eta} + \frac{\upsilon\bar{\omega}}{\eta} \quad (47)$$

4.5 Undrained condition

For undrained expansion of a cylindrical cavity, the volumetric strain rate $\tilde{\varepsilon}_v$ vanishes everywhere around the cavity, i.e.,

$$\tilde{\varepsilon}_v = -\frac{\tilde{\upsilon}}{\upsilon} = 0 \quad (48)$$

Hence, applying Eq. (13) to (48), the undrained condition in terms of the dimensionless form can be given as

$$\frac{d\boldsymbol{\upsilon}}{d\eta} = 0 \quad (49)$$

5. Coupled governing equations

The governing equations for the problem considered can be formulated by combining the equilibrium equation Eq.

1. **Data:** initial stress state, model parameters and cavity expansion radius ratio
2. Determining the non-dimensionalized stress components, hardening parameter, specific volume, pore water pressure and particle velocity at EP boundary ($\sigma_r'(r_p)$, $\sigma_\theta'(r_p)$, $\sigma_z'(r_p)$, $p_c'(r_p)$, $\upsilon(r_p)$ and $\omega(r_p)$)
3. Determining the position of EP boundary (r_p)
4. Introducing the dimensionless radial coordinate ($\eta = r/r_p$) and converting the variable interval $r = (r_p, a)$ to $\eta = (\eta_p, \eta_a)$
5. Determining the initial values at the EP boundary with η_p ($\sigma_r'(\eta_p)$, $\sigma_\theta'(\eta_p)$, $\sigma_z'(\eta_p)$, $p_c'(\eta_p)$, $\upsilon(\eta_p)$ and $\omega(\eta_p)$)
6. Setting a vector $\eta_r = \text{linspace}(\eta_p, \eta_a, m)$. Note that the value of m here should be large enough.
7. **For** $i = 1{:}\,m-1$

   Solving the governing equation group in the plastic region:
   $[T, Y] = \text{ode45}(@similar, [1\ entar], [\sigma_r'(r_p), \sigma_\theta'(r_p), \sigma_z'(r_p), p_c'(r_p), \upsilon(r_p), \omega(r_p)])$

   Function $dy = similar(s, y)$

   7.1 Obtaining $s = [\eta_p, \eta_r(i)]$ and $y =], [\sigma_r'(r_p), \sigma_\theta'(r_p), \sigma_z'(r_p), p_c'(r_p), \upsilon(r_p), \omega(r_p)]$

   7.2 Computing the elements of the coefficient matrix on the left-hand side of Eq. (50)

   7.3 Calculating $d\sigma_r'/dr$, $d\sigma_\theta'/dr$, $d\sigma_z'/dr$, dp_c'/dr, $d\upsilon/dr$ and $d\omega/dr$

   End function
8. Obtaining $\sigma_r'(\eta_r(i))$, $\sigma_\theta'(\eta_r(i))$, $\sigma_z'(\eta_r(i))$, $p_c'(\eta_r(i))$, $\upsilon(\eta_r(i))$, $\omega(\eta_r(i))$

   End
9. Getting $\sigma_r'(\eta_r)$, $\sigma_\theta'(\eta_r)$, $\sigma_z'(\eta_r)$, $p_c'(\eta_r)$, $\upsilon(\eta_r)$, $\omega(\eta_r)$.
10. Converting the solution for the seven variables to the form under the radial coordinate $\sigma_r'(r)$, $\sigma_\theta'(r)$, $\sigma_z'(r)$, $p_c'(r)$, $\upsilon(r)$, $\omega(r)$
11. Calculating the stress components in the elastic zone

Fig. 3 Flowchart of the solution procedure for determining stress distributions during cavity expansion

(15), the constitutive equations Eqs. (37)-(39), the consistency condition Eq. (44), the continuity condition Eq. (47) and the undrained condition Eq. (49), which can be written in the matrix form as

$$\begin{bmatrix} 1 & 0 & 0 & 0 & 1 & 0 & 0 \\ \beta\bar{A}_r & \beta\bar{A}_\theta & \beta\bar{A}_z & 0 & 0 & 0 & 1 \\ \beta\bar{B}_r & \beta\bar{B}_\theta & \beta\bar{B}_z & 0 & 0 & 0 & 0 \\ \bar{C}_r & \bar{C}_\theta & \bar{C}_z & 0 & 0 & 0 & 0 \\ \bar{D}_r & \bar{D}_\theta & \bar{D}_z & -1/\bar{p}' & 0 & 0 & 0 \\ 0 & 0 & 0 & 0 & 0 & \beta & -\upsilon \\ 0 & 0 & 0 & 0 & 0 & 1 & 0 \end{bmatrix} \begin{bmatrix} d\bar{\sigma}_r'/d\eta \\ d\bar{\sigma}_\theta'/d\eta \\ d\bar{\sigma}_z'/d\eta \\ d\bar{p}_c'/d\eta \\ d\bar{u}/d\eta \\ d\upsilon/d\eta \\ d\bar{\omega}/d\eta \end{bmatrix} = \begin{bmatrix} -(\bar{\sigma}_r' - \bar{\sigma}_\theta')/\eta \\ 0 \\ -\bar{\omega}/\eta \\ 0 \\ 0 \\ \upsilon\bar{\omega}/\eta \\ 0 \end{bmatrix} \tag{50}$$

Now, the governing equations for the problem considered have been formulated as a system of first-order ordinary differential equations. Since all the seven basic unknowns are involved in formulating the governing equations for the problem considered, the present similarity solution has the advantage of being more generic than the solution of Li *et al.* (2016) as only three unknowns are involved in their solution. However, it should be noted that the model will become not flexible, which requires larger computational cost, as more variables are involved in the proposed solution. Since the cavity expands in a self-similar manner, the governing equations can be readily solved as an initial value problem if the initial values of the basic state variables are determined. In this study, the governing equations are solved by making use of the ODE45 solver of MATLAB package. The flowchart shown by Fig. 3 gives the solution procedure for determining stress distributions in soils during cavity expansion. It is believed that such a scheme could help readers figure out the codes very quickly.

6. Initial values for solving governing equations

6.1 Elastic analysis

Combining the equilibrium equation, the small strain theory and Hooke's law, the elastic solution for cylindrical cavity expansion can be given as follows according to Li *et al.* (2016)

$$\sigma_r' = \sigma_{h0}' + (\sigma_{rp}' - \sigma_{h0}')(\frac{r_p}{r})^2 \tag{51}$$

$$\sigma_\theta' = \sigma_{h0}' - (\sigma_{rp}' - \sigma_{h0}')(\frac{r_p}{r})^2 \tag{52}$$

$$\sigma_z' = \sigma_{v0}' \tag{53}$$

$$\Delta u = 0 \tag{54}$$

$$U_r = \frac{\sigma_{rp}' - \sigma_{h0}'}{2G_0}\frac{r_p^2}{r} \tag{55}$$

where G_0 is the initial shear modulus; σ_{rp}' denotes the effective radial stress at the elastic-plastic boundary.

6.2 Initial values of state variables

The initial values of the state variables required for solving the governing equations should be the values of the basic unknowns at the instant the soil become plastic state. As indicated by Li *et al.* (2016), the dimensionless effective radial, circumferential and vertical stresses as well as the particle displacement at the elastic-plastic boundary are independent of the radial coordinate and can be given as

$$\bar{\sigma}'_{\mathrm{rp}} = \bar{\sigma}'_{\mathrm{h0}} + \frac{\sqrt{3}}{3}\bar{\mathrm{p}}'_0 \mathrm{M}^* \sqrt{\mathrm{OCR}-1} \tag{56}$$

$$\bar{\sigma}'_{\theta\mathrm{p}} = \bar{\sigma}'_{\mathrm{h0}} - \frac{\sqrt{3}}{3}\bar{\mathrm{p}}'_0 \mathrm{M}^* \sqrt{\mathrm{OCR}-1} \tag{57}$$

$$\bar{\sigma}'_{\mathrm{zp}} = \bar{\sigma}'_{\mathrm{z0}} = \frac{3\bar{\mathrm{p}}'_0}{1+2\mathrm{K}_0} \tag{58}$$

where OCR is the overconsolidation ratio.

Based on Eq. (8), the initial value of the dimensionless particle velocity can be given as

$$\bar{\omega}_{\mathrm{p}} = \frac{\omega_{\mathrm{p}}}{\mathrm{W}} = \frac{\mathrm{dU_r}}{\mathrm{dr}}|_{\mathrm{r=r_p}} = \frac{\sqrt{3}}{3\bar{\mathrm{G}}_0}\bar{\mathrm{p}}'_0 \mathrm{M}^* \sqrt{\mathrm{OCR}-1} \tag{59}$$

where $\bar{\mathrm{G}}_0 = \mathrm{G}_0/\mathrm{p}'_1$ is the dimensionless initial shear modulus.

Since the volume of the soil keeps constant during the undrained expansion, the specific volume at the elastic-plastic boundary, υ_p, can be directly given as

$$\upsilon_p = \upsilon_0 \tag{60}$$

It can be seen from Eq. (54) that no excess pore water pressure is generated in the elastic region, hence the pore water pressure at the elastic-plastic boundary can be deduced from the continuity condition as follows

$$u_p = u_0 \tag{61}$$

The initial value of the hardening parameter, $\bar{\mathrm{p}}'_{\mathrm{c0}}$, can be calculated from Eq. (1) as follows

$$\bar{p}'_{\mathrm{c0}} = \mathrm{OCR} \times \bar{p}'_0 \left(1 + \frac{\eta_0^2}{M^{*2}}\right) \tag{62}$$

Now, all the initial values of the basic variables have been determined, and hence the governing equations are readily to be solved. It should be noted that the results from the governing equations are presented in terms of the dimensionless coordinate η rather than the real radial coordinate r. The dimensionless coordinate can be related to the real radial coordinate in the following.

Since the volumetric strain remains zero during the undrained expansion process, the radial coordinate of an arbitrary soil particle r_x during cavity expansion can be related to the cavity radius as follows

$$r_x^2 - r_{x0}^2 = a^2 - a_0^2 \tag{63}$$

where r_{x0} denotes the initial radial coordinate of the particle considered; a and a_0 are the current cavity radius and the initial cavity radius, respectively.

From Eq. (55), the radial displacement of the soil particle at the elastic-plastic boundary can be given as

$$\mathrm{U_{rp}} = \mathrm{r_{xp}} - \mathrm{r_{x0}} = \frac{\sigma'_{\mathrm{rp}} - \sigma'_{\mathrm{h0}}}{2\mathrm{G}_0}\mathrm{r_{xp}} \tag{64}$$

Combining Eqs. (63) and (64), the radius of the plastic region $\mathrm{r_p}$ can be determined as

$$r_{\mathrm{p}} = 2G_0 \sqrt{\frac{a_0^2 - a^2}{\left[2G_0 - (\sigma'_{\mathrm{rp}} - \sigma'_{\mathrm{h0}})\right]^2 - 4G_0^2}} \tag{65}$$

Based on the definition of the dimensionless radial coordinate η and Eq. (65), the real radial coordinate can be related to η as follows

$$r = \eta r_p = 2G_0\eta \sqrt{\frac{a_0^2 - a^2}{\left[2G_0 - (\sigma'_{rp} - \sigma'_{h0})\right]^2 - 4G_0^2}} \tag{66}$$

7. Validation and discussion

7.1 Comparison with previous solutions

To validate the present similarity solution, the expansion responses and the distributions of the stresses calculated from the proposed solution will be compared with the rigorous solutions of Chen and Abousleiman (2012) and Li *et al.* (2016). The soil parameters used in the calculation are the same as those employed in Li *et al.* (2016), which are summarized in Table 2. It should be clarified that rigorous solution of Li *et al.* (2016) also used the K_0-AMCC model, and hence the comparisons with the results from Li *et al.* (2016) could directly reflect the validity of the proposed genetic similarity solution. The rigorous solution of Chen and Abousleiman (2012) is based on the MCC model, thus the comparisons with the MCC model based solution of (2012) will show the impacts of soil anisotropy on the cavity expansion responses.

The distributions of the three stress components around the cavity at the instant cavity radius $a/a_0 = 2$ for different OCRs are plotted in Fig. 4(a)-4(d). The results of both Chen and Abousleiman (2012) and Li *et al.* (2016) are included for comparison. It can be observed that for normally consolidated clay, no elastic region exists around the cavity because the soil instantly comes into the plastic state as long as the cavity begins to expand, which can be well explained by Eq. (56). It can be seen from Fig. 4 that the proposed solution perfectly overlaps the rigorous solution of Li *et al.* (2016), which manifests the validity of the present similarity solution. Comparing the results with the isotropic solution of Chen and Abousleiman (2012), it can be found that the stress components are more or less overestimated or underestimated by the isotropic solution except for the case of K_0=1, which highlights the significant effects of soil anisotropy on the cavity expansion responses.

Table 2 Initial parameters and soil properties for calculation

OCR	σ'_{r0} /kPa	$\sigma'_{\theta 0}$ /kPa	σ'_{z0} /kPa	u_0/kPa	K_0	υ_0	G_0 /kPa
1	100	100	160	100	0.625	2.09	4357
1.2	100	100	160	100	0.625	2.06	4294
3	120	120	120	100	1	1.97	4106
10	144	144	72	100	2	1.8	3752

$M = 1.2, \kappa = 0.03, \lambda = 0.15, v = 0.278, v_{cs} = 2.74$

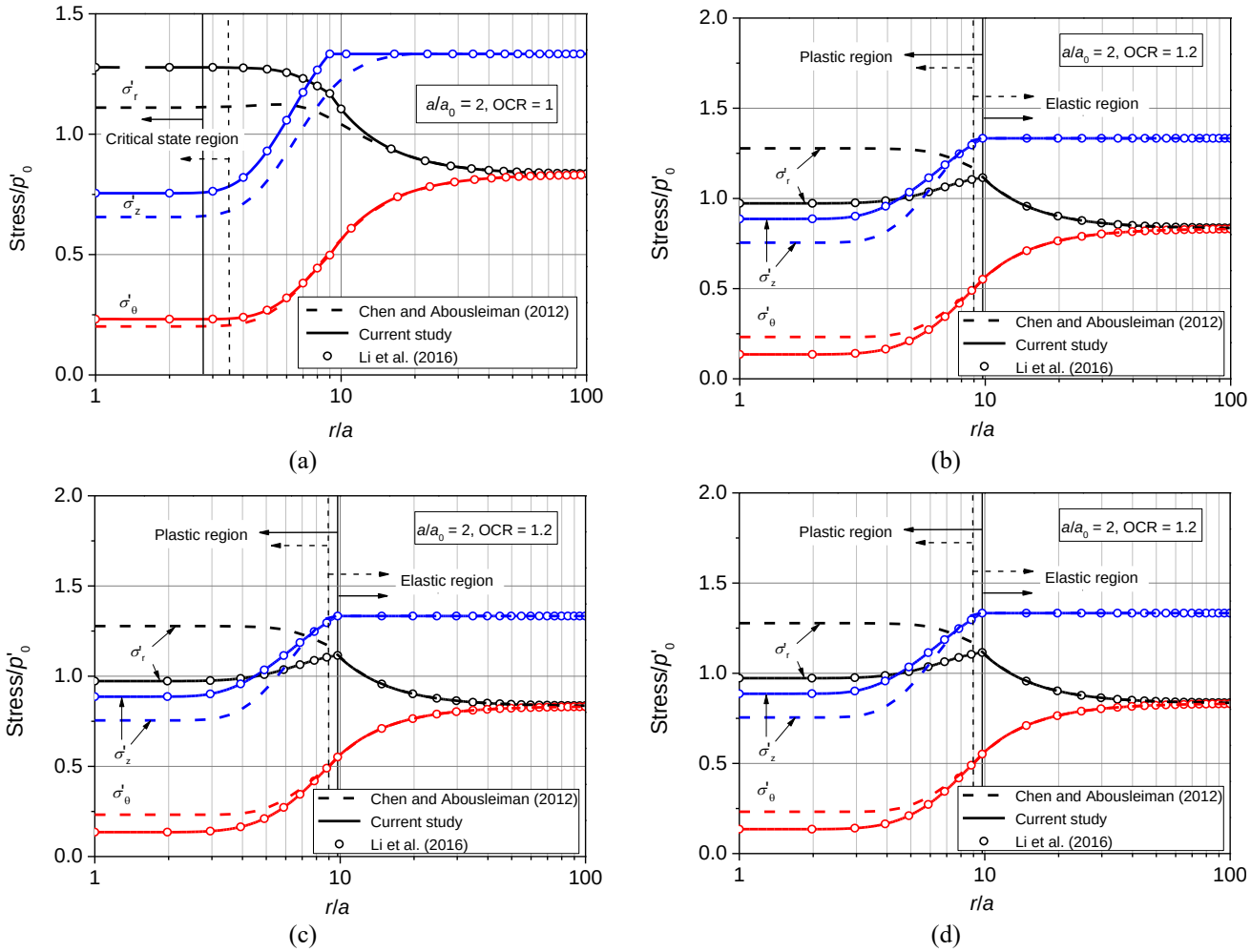

Fig. 4 Distributions of stress components around cavity: (a) OCR=1, K_0=0.625, (b) OCR=1.2, K_0=0.625, (c) OCR=3, K_0=1 and (d) OCR=10, K_0=2

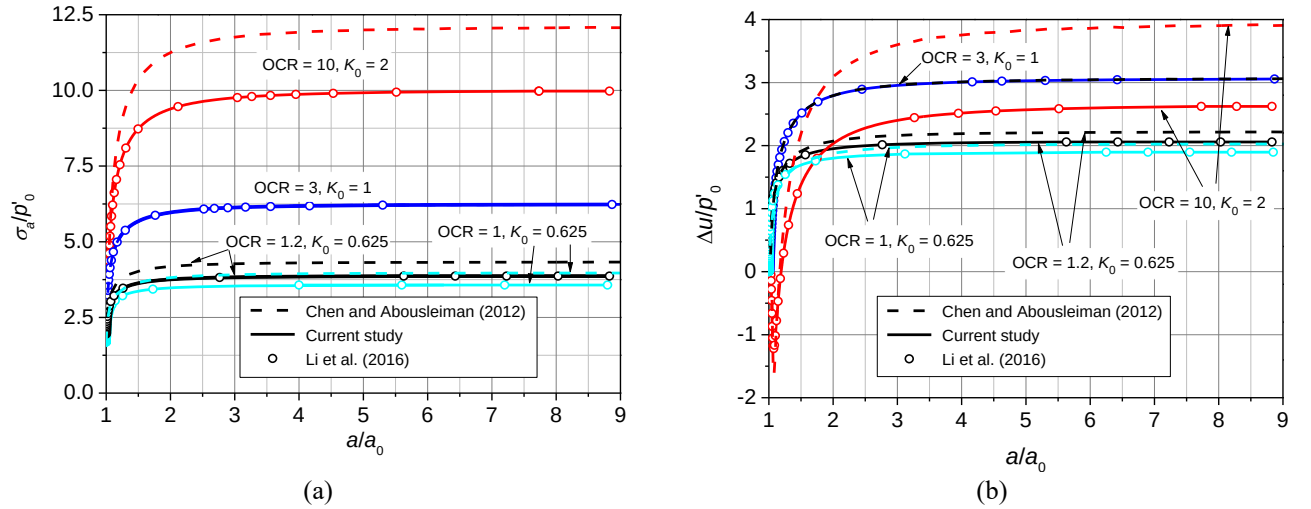

Fig. 5 Development of expansion pressure and excess pore pressure at cavity wall during cavity expansion: (a) expansion pressure and (b) excess pore pressure

Figs. 5(a) and 5(b) display the variations of the internal expansion pressure and the excess pore pressure developed at the cavity wall from $a/a_0 = 0$ to $a/a_0 = 10$, respectively. The results of Chen and Abousleiman (2012) and Li *et al.* (2016) are also included for comparison. It can be easily discerned from Fig. 5 that the expansion pressure at the cavity wall increase rapidly when $a/a_0 < 3$, after that the internal expansion pressure increase insignificantly

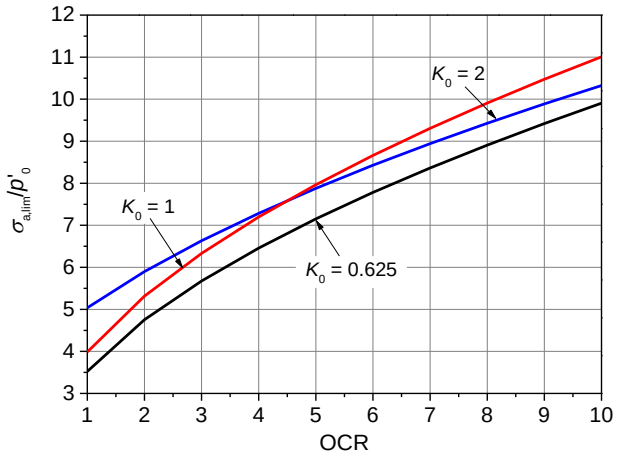

Fig. 6 Variation of ultimate expansion pressure with overconsolidation ratio for different coefficients of earth pressure at rest

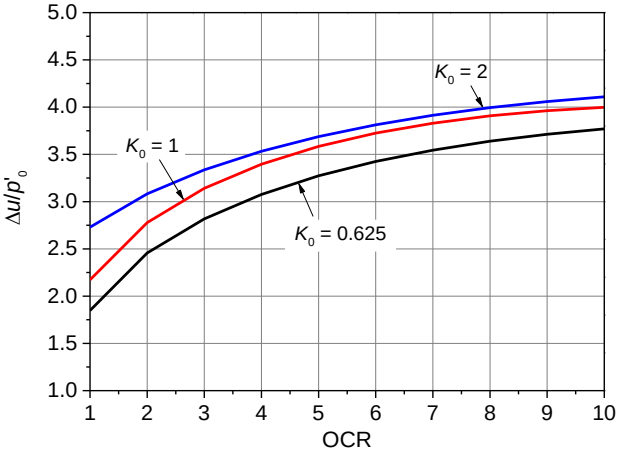

Fig. 7 Variation of ultimate excess pore pressure at cavity wall with overconsolidation ratio for different coefficients of earth pressure at rest

with further expansion of the cavity. Finally, the expansion pressure reaches a limit value when the soil at the cavity wall reaches the critical state. It can be found that the expansion pressures from the present similarity solution agree fairly well with the solution of Li *et al.* (2016), which again demonstrates the validation of the proposed solution. However, the isotropic solution of Chen and Abousleiman (2012) greatly overestimated the cavity expansion pressure and the excess pore water pressures at the cavity wall other than the case K_0=1. This means the isotropic solution might yield progressive predictions when it is applied to the anisotropic soils. Further inspection of the figure, it can be found that the difference between the anisotropic solution and isotropic solution increases as the overconsolidation ratio increases, which illustrates that the error of MCC model based isotropic solution will increase with the overconsolidation ratio.

It should be noted that since only three stress components are considered in the solution of Li *et al.* (2016), the hardening parameter cannot be obtained from the solution of Li *et al.* (2016). Therefore, the yield loci of the soil around the cavity are absent in their study, which

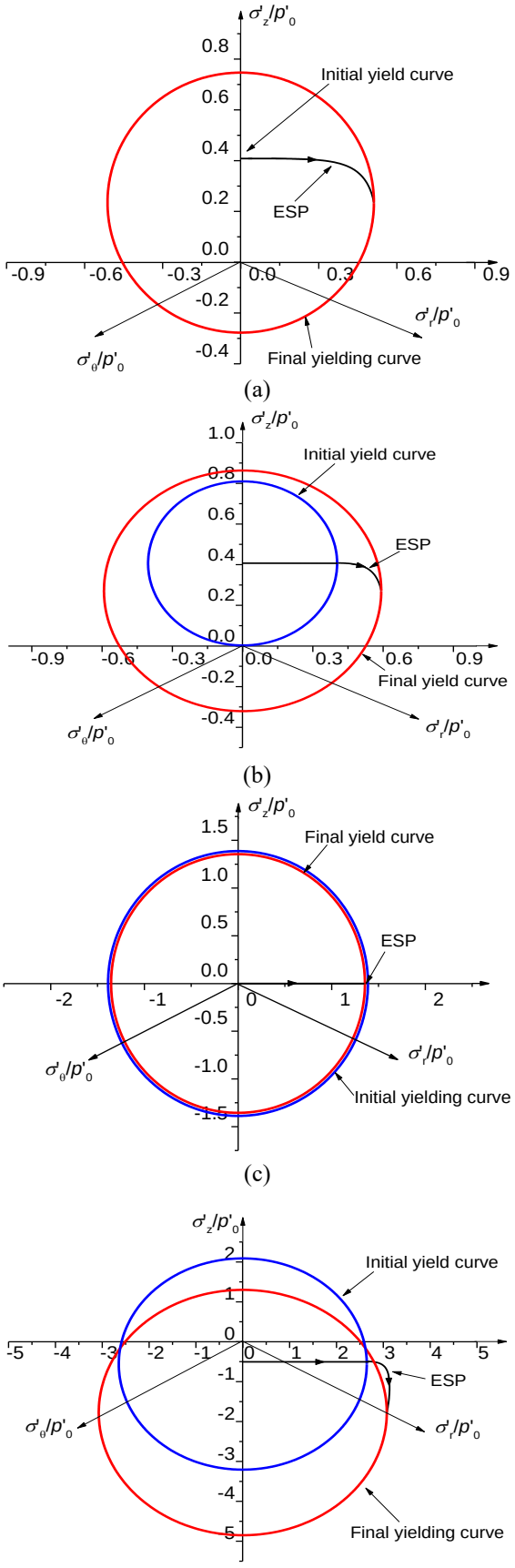

Fig. 8 Stress paths in π plane for a soil particle at cavity wall: (a) OCR=1, K_0=0.625m (b) OCR=1.2, K_0=0.625, (c) OCR=3, K_0=1 and (d) OCR=10, K_0=2

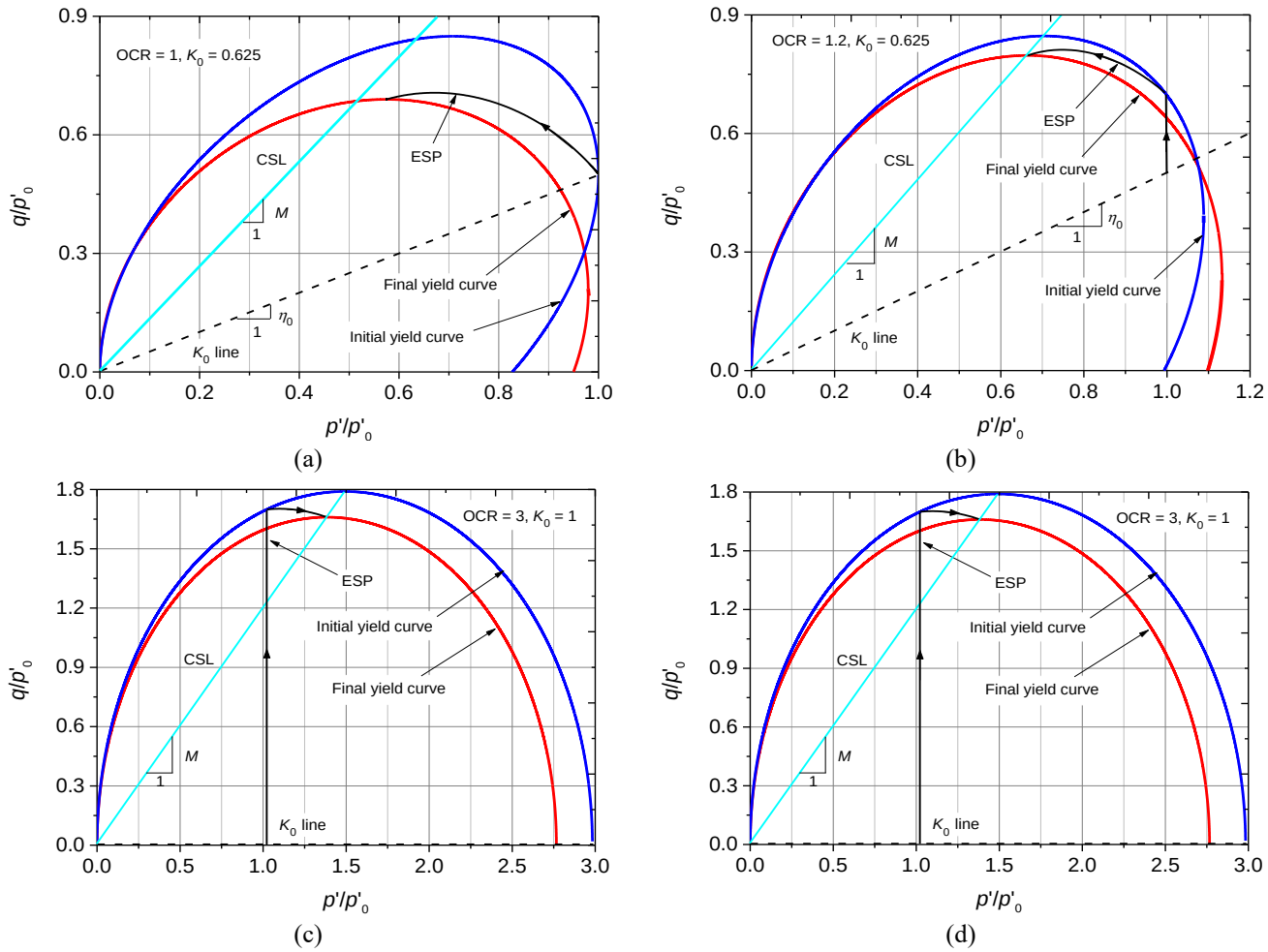

Fig. 9 Stress paths in p'–q plane for a soil particle at cavity wall: (a) OCR=1, K_0=0.625, (b) OCR=1.2, K_0=0.625, (c) OCR=3, K_0=1 and (d) OCR=10, K_0=2

well demonstrates the generality and advantage of the proposed solution.

Figs. 6 and 7 show the variations of the ultimate expansion pressure and excess pore pressure at the cavity wall with the overconsolidation ratio for different coefficients of earth pressure at rest, respectively. It can be seen from Figs. 6 and 7 that both the limit expansion pressure and the excess pore pressure at the cavity wall increase as overconsolidation ratio increases. These two phenomena can be explained by the fact that the strength and stiffness of the soil increase with the overconsolidation ratio. Hence, larger expansion pressure is required to expand the cavity as the consolidation ratio increases and larger excess pore pressure will be generated during the cavity expansion process.

Figs. 8(a)-8(d) display the projections of the stress paths of a soil particle at the cavity wall during cavity expansion and the evolutions of the projections of the yield surface in the π plane. As seen in the figure, the yield locus in π plane deviate from the origin of the coordinate other than the case of $K_0 = 1$ because of the initial stress anisotropy. The projections of the stress paths departure from z axis and move right to approach the finial yield surface during the cavity expansion process. Since the vertical effective stress σ_z' remains unchanged during the cavity expansion process, the stress path shows as a horizontal straight line during the elastic process. When the soil becomes plastic state, the projection of the stress path turns down and moves right until reaches the finial yield surface, this is because the radial effective stress σ_r' increases, the tangential effective stress σ_θ' and the vertical effective stress σ_z' decrease after yielding of the soil. For the isotropic soil with $K_0 = 1$, the projection of the stress path always remains as a horizontal straight line during the whole cavity expansion process, as the vertical effective stress is equal to the average of the radial effective stress and tangential effective stress during both elastic and plastic expansion processes.

Figs. 9(a)-9(d) plot the stress paths and the corresponding projection of the yield surface for different OCRs in $p' - q$ plane. It should be noted that the yield curves are the projection of the yield surface passing through the stress point, which are plotted according to the Lode's angle and the soil stress state. As seen in the figure, all the stress paths (except for the case of K_0=1) start from the K_0 line and moves up vertically before touching the initial yield surface. Then, the stress paths turn left for slightly overconsolidated soil or right for heavily overconsolidated soil to approach the critical state line,

Table 3 Physical and mechanical properties of soil

Soil properties	Value
Effective unit weight γ'(kN/m^3)	8.75
Effective internal frictional angle φ'(°)	30
Coefficient of earth pressure at rest K_0	0.55
OCR	1.0
Horizontal coefficient of permeability k_h(m/s)	2.65×10^{-7}
Initial void ratio e_0	0.98
Slope of loading line λ	0.11
Slope of unloading-reloading line κ	0.02

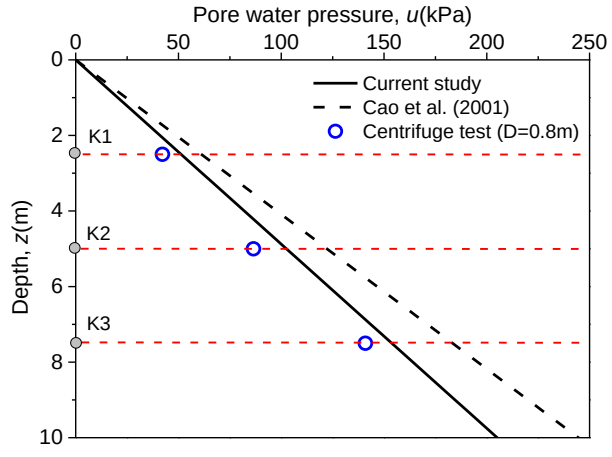

Fig. 10 Comparison of pore water pressure at different depths among current study, previous study and measured results

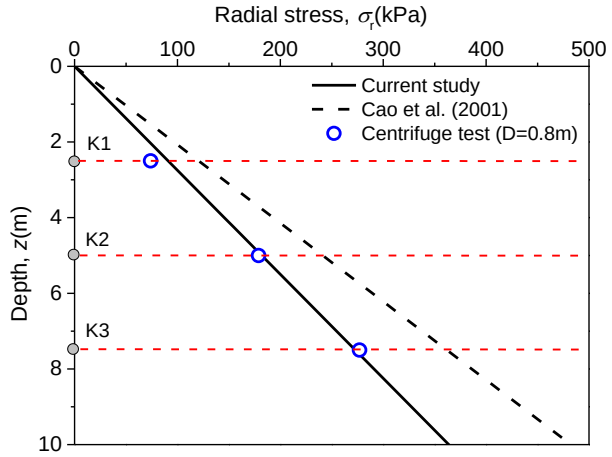

Fig. 11 Comparison of radial stress at different depths among current study, previous study and measured results

which corresponds to the hardening or softening behaviors of the soil after plastic yielding. This well reflects the strain hardening behavior of the normally consolidated and lightly overconsolidated soils, while strain softening behavior of the overconsolidated soils during cavity expansion process. It also interesting to observe that the projection of the yield surface is a standard ellipse in $p'-q$ plane for the isotropic soil with K_0=1, while projections of the yield surfaces are distorted and rotated ellipses in $p'-q$ plane for anisotropic soils. The declination of the yield loci decreases at the finial state, which reflects the changes in the stress anisotropy of the soil due to the cavity expansion effects.

7.2 Comparison with centrifuge model test

To demonstrate the application of the present method, the proposed solution is applied to predicting a centrifuge model test for jacked pile installation. The centrifuge model tests chosen for comparison were conducted on TLJ-150 centrifuge at Tongji University by Li *et al.* (2016). Since the displacement of soil around the pile shaft during pile installation is extremely similar to that around an expanding cavity, the comparison could manifest the validity and practicability of the proposed solution.

The aluminum alloy piles, with a diameter of 1.6 cm, were used as model piles in the centrifuge model test. According to the scale factors of centrifuge model test, it is not hard to know that the model piles correspond to the prototype piles with a diameter of 0.8 m in practical engineering. The embedment depth of the piles was designed to be 10 m with the pore pressure transducers and the earth pressure transducers being located at the depth of 2.5 m, 5 m and 7.5 m, respectively, and 0.8 m away from the pile center in radial direction. Hence, in the centrifuge model scale, the model piles were penetrated into the soil for 200 mm and the transducers were installed at the depth of 50 mm, 100 mm and 150 mm, respectively, and 16 mm away from the center of the model pile, which were fixed in the soil with the aid of aluminum bars. A displacement-control motor was utilized to jack the model piles into soil at a constant rate of 9 cm/min, which ensured the undrained condition during pile installation.

The silty clay used in the centrifuge test was obtained from the fifth stratum of Shanghai. The soil sample was first dried and smashed into particles and then mixed with water in a vacuum stirring tank to form saturated slurry in terms of the moisture content at saturated state. Subsequently, the slurry was poured into the model container with a size of 600 mm × 400 mm × 400 mm and consolidated for 10 h at a centrifugal acceleration of 50 g to gain initial strength. The physical and mechanical properties of the soil used in the test are listed in Table 3 based on results of laboratory tests. More detailed information regarding the centrifuge model tests can be found in Li *et al.* (2016), and hence is not further introduced here.

Figs. 10 and 11 show the comparison of pore water pressure and radial stress among the present solution, the previous isotropic solution of Cao *et al.* (2001) and the measured data from the centrifuge test, respectively. It should be noted that the measured results are transformed and expressed as prototype scale in Figs. 9 and 10 so as to directly show the performance of the proposed method in practical engineering. It can be clearly seen from Figs. 10 and 11 that both the pore water pressure and the radial stress increase substantially with the increase of depth. Since the strength and the stiffness of the soil are proportional to the effective stress, which increases linearly with depth, larger

expansion pressure is required to expand the cavity and higher excess pore water pressure will be generated for the deeper soil. It should also be noted that the isotropic closed-form solution developed by Cao *et al.* (2001) overestimates the pore water pressure and the radial stress compared with the present anisotropic solution, which sufficiently illustrates that the present anisotropic solution could yield more accurate predictions than the MCC based isotropic solutions when analyzing the practical engineering problem.

8. Conclusions

In this study, a generic similarity solution is developed for cylindrical cavity expansion in K_0-consolidated anisotropic soils under undrained condition. The solution properly considers the effects of the initial stress anisotropy and the stress-induced anisotropy of the soil during cavity expansion. It should be noted that an auxiliary variable could be introduced to enable application of the proposed solution to drained or partially drained cavity expansion problems, as mentioned in Li *et al.* (2017). Some main conclusions are summarized as follows:

(a) The present similarity solution for cavity expansion in anisotropic soils perfectly matches with the rigorous solution of Li *et al.* (2016), but the present solution is more standard and generic than that of Li *et al.* (2016) as all the unknown variables are involved in formulating the governing equation group.

(b) The isotropic solution overestimates the expansion pressure other than K_0=1, and the overestimation increases as the overconsolidation ratio increases, which demonstrates that the anisotropy and the overconsolidation ratio have significant effects on the expansion responses.

(c) The present similarity solution shows more accurate predictions of pore water pressure and radial stress than the isotropic solutions, which demonstrates the significant effect of soil anisotropy on the expansion responses.

Acknowledgments

This study is financially supported by the National Natural Science Foundation of China (Grant No. 41772290).

References

Cao, L.F., Teh, C.I. and Chang, M.F. (2001), "Undrained cavity expansion in modified Cam clay I: Theoretical analysis", *Géotechnique*, **51**(4), 323-334. https://doi.org/10.1680/geot.2001.51.4.323.

Carter, J.P., Booker, J.R. and Yeung, S.K. (1986), "Cavity expansion in cohesive frictional soils", *Géotechnique*, **36**(3), 349–358. https://doi.org/10.1680/geot.1986.36.3.349.

Chang, M.F., Teh, C.I. and Cao, L.F. (2001), "Undrained cavity expansion in modified Cam clay II: Application to the inter*pr*etation of the piezocone test", *Géotechnique*, **51**(4), 335-350. https://doi.org/10.1680/geot.2001.51.4.335.

Chen, H.H., Li, L., Li, J.P. and Wang, H. (2019), "Stress transform method to undrained and drained expansion of a cylindrical cavity in anisotropic modified cam-clay soils", *Comput. Geotech.*, **106**, 128-142. https://doi.org/10.1016/j.compgeo.2018.10.016.

Chen, S.L. and Abousleiman, Y.N. (2012), "Exact undrained elasto-plastic solution for cylindrical cavity expansion in modified Cam Clay soil", *Géotechnique*, **62**(5), 447-456. https://doi.org/10.1680/geot.11.P.027.

Chen, S.L. and Liu, K. (2018), "Undrained cylindrical cavity expansion in anisotropic critical state soils", *Géotechnique*, **69**(3), 189-202. https://doi.org/10.1680/jgeot.16.p.335.

Collins, I.F. and Stimpson, J.R. (1994), "Similarity solutions for drained and undrained cavity expansions in soils", *Géotechnique*, **44**(1), 21-34. https://doi.org/ 10.1680/geot.1994.44.1.21.

Cudmani, R. and Osinov, V.A. (2001), "The cavity expansion problem for the interpretation of cone penetration and pressuremeter tests", *Can. Geotech. J.*, **38**(3), 622-638. https://doi.org/10.1139/t00-124.

Dafalias, Y.F. (1986), "An anisotropic critical state soil plasticity model", *Mech. Res. Commun.*, **13**(6), 341-347. https://doi.org/10.1016/0093-6413(86)90047-9.

dos Santos, T., Vaz-Romero, A. and Rodríguez-Martínez, J.A. (2019), "Dynamic cylindrical cavity expansion in orthotropic porous ductile materials", *Int. J. Impact Eng.*, **132**, 103325. https://doi.org/10.1016/j.ijimpeng.2019.103325.

Gao, Y., Li, Z., Sun, D.A. and Yu, H.H. (2021), "A simple method for predicting the hydraulic properties of unsaturated soils with different void ratios", *Soil Till. Res.*, **209**, 104913. https://doi.org/10.1016/j.still.2020.104913.

Houlsby, G.T. and Withers, N.J. (1988), "Analysis of the cone pressuremeter test in clay", *Géotechnique*, **38**(4), 575-587. https://doi.org/10.1680/geot.1988.38.4.575.

Johnsen, J., Holmen, J.K., Warren, T.L. and Borvik, T. (2018), "Cylindrical cavity expansion approximations using different constitutive models for the target material", *Int. J. Protective Struct.*, **9**(2), 199-225. https://doi.org/10.1177%2F2041419617741321.

Ladanyi, B. (1963), "Expansion of a cavity in a saturated clay medium", *J. Soil Mech. Found. Div.*, **89**(4), 127-164.

Li, C. and Zou, J.F. (2019), "Closed-form solution for undrained cavity expansion in anisotropic soil mass based on spatially mobilized plane failure criterion", *Int. J. Geomech.*, **19**(7), 04019075. https://doi.org/10.1061/(ASCE)GM.1943-5622.0001458.

Li, J.P., Gong, W.B., Li, L. and Liu, F. (2017), "Drained elastoplastic solution for cylindrical cavity expansion in K_0-consolidated anisotropic soil", *J. Eng. Mech.*, **143**(11), 04017133. https://doi.org/10.1061/(ASCE)em.1943-7889.0001357.

Li, L., Chen, H.H., Li, J.P. and Sun, D.A. (2021), "An elastoplastic solution to undrained expansion of a cylindrical cavity in SANICLAY under plane stress condition", *Comput. Geotech.*, **132**: 103990. https://doi.org/10.1016/j.compgeo.2020.103990.

Li, L., Li, J.P. and Sun, D.A. (2016), "Anisotropically elasto-plastic solution to undrained cylindrical cavity expansion in K_0-consolidated clay", *Comput. Geotech.*, **73**, 83-90. https://doi.org/10.1016/j.compgeo.2015.11.022.

Marshall, A.M. (2012), "Tunnel-pile interaction analysis using cavity expansion methods", *J. Geotech. Geoenviron. Eng.*, **138**(10), 1237-1246. https://doi.org/10.1061/(ASCE)GT.1943-5606.0000709.

Matsuoka, H. and Sun, D.A. (2014), *The SMP Concept-Based 3D Constitutive Models for Geomaterials*, CRC Press.

Mo, P.Q., Gao, X.W., Yang, W.B. and Yu, H.S. (2020a), "A cavity expansion–based solution for interpretation of CPTu data in soils under partially drained conditions", *Int. J. Numer. Anal. Met.*, **44**(7), 1053-1076. https://doi.org/10.1002/nag.3050.

Mo, P.Q., Ma, D.Y., Zhu, Q.Y. and Hu, Y.C. (2020b), "Interpretation of heating and cooling data from thermal cone penetration test using a 1D numerical model and a PSO algorithm", *Comput. Geotech.*, **130**, 103908. https://doi.org/10.1016/j.compgeo.2020.103908.

Mo, P.Q., Marshall, A.M. and Fang, Y. (2021), "Cavity expansion–contraction-based method for tunnel-soil-pile interaction in a unified clay and sand model: drained analysis", *Int. J. Geomech.*, **21**(5), 04021055. https://doi.org/10.1061/(ASCE)GM.1943-5622.0002016.

Moug, D.M., Boulanger, *R*.W, DeJong, J.T. and Jaeger, R.A. (2019), "Axisymmetric simulations of cone penetration in saturated clay", *J. Geotech. Geoenviron. Eng.*, **145**(4), 04019008. https://doi.org/10.1061/(asce)gt.1943-5606.0002024.

Peng, Y., Liu, H.L., Li, C., Ding, X.M., Deng, X., and Wang, C.Y. (2021), "The detailed particle breakage around the pile in coral sand", *Acta Geotech.*, https://doi.org/10.1007/s11440-020-01089-2.

Randolph, M.F., Carter, J.P. and Wroth, C.P. (1979), "Driven piles in clay—the effects of installation and subsequent consolidation", *Géotechnique*, **29**(4), 361-393. https://doi.org/10.1680/geot.1979.29.4.361.

Roscoe, K.H. and Burland, J.B. (1968), *On the Generalized Stress-Strain Behavior of 'Wet Clay'*, Cambridge University Press.

Russell, A.R. and Khalili, N. (2002), "Drained cavity expansion in sands exhibiting particle crushing", *Int. J. Numer. Anal. Met.*, **26**(4), 323-340. https://doi.org/10.1002/nag.203.

Salgado, R., Mitchell, J.K. and Jamiolkowski, M. (1997), "Cavity expansion and penetration resistance in sand", *J. Geotech. Geoenviron. Eng.*, **123**(4), 344-354. https://doi.org/10.1061/(ASCE)1090-0241(1997)123:4(344).

Sekiguchi, H. and Ohta, H. (1977), "Induced anisotropy and time dependency in clays", *Proceedings of the 9th ICSMFE*, Tokyo, Japan, July.

Silvestri, V. and Abou-Samra, G. (2012), "Analytical solution for undrained plane strain expansion of a cylindrical cavity in modified cam clay", *Geomech. Eng.*, **4**(1), 19-37. https://doi.org/10.12989/gae.2012.4.1.019.

Sivasithamparam, N. and Castro, J. (2018), "Undrained expansion of a cylindrical cavity in clays with fabric anisotropy: Theoretical solution", *Acta Geotech.*, **13**(3), 729-746. https://doi.org/10.1007/s11440-017-0587-4.

Vrakas, A. (2016), "A rigorous semi-analytical solution for undrained cylindrical cavity expansion in critical state soils", *Int. J. Numer. Anal. Met.*, **40**(15), 2137-2160. https://doi.org/10.1002/nag.2529.

Wang, Y., Li, L., Li, J.P. and Sun, D.A. (2020), "Jet-grouting in ground improvement and rotary grouting pile installation: Theoretical analysis", *Geomech. Eng.*, **21**(3), 279-288. https://doi.org/10.12989/gae.2020.21.3.279.

Wheeler, S.J., Näätänen, A., Karstunen, M. and Lojander, M. (2003), "An anisotropic elastoplastic model for soft clays", *Can. Geotech. J.*, **40**(2), 403-418. https://doi.org/10.1139/t02-119.

Wroth, C.P. and Windle, D. (1975), "Analysis of the pressuremeter test allowing for volume change", *Géotechnique*, **25**(3), 598-604. https://doi.org/10.1680/geot.1975.25.3.598.

Yang, C.Y., Chen, H.H. and Li, J.P. (2020), "Drained cylindrical cavity expansion analysis in anisotropic soils considering 3D strength", *Geotechnique Lett.*, **10**(2), 346-352. https://doi.org/10.1680/jgele.19.00043.

Yang, C.Y., Li, J.P., Li, L. and Sun DA. (2021a), "Expansion responses of a cylindrical cavity in overconsolidated unsaturated soils: A semi-analytical elastoplastic solution", *Comput. Geotech.*, **130**, 103922. https://doi.org/10.1016/j.compgeo.2020.103922.

Yang, C.Y., Chen, H.H., Li, J.P. and Li, L. (2021b), "Undrained spherical cavity expansion in unsaturated soils: Semi-analytical solution coupling hydraulic and mechanical behaviors", *Int. J. Geomech.*, **21**(6), 04021070. https://doi.org/10.1061/(ASCE)GM.1943-5622.0002028.

Zhou, H., Kong, G.Q. and Liu, H.L. (2016), "A semi-analytical solution for cylindrical cavity expansion in elastic–perfectly plastic soil under biaxial in situ stress field", *Géotechnique*, **66**(7), 1-12. https://doi.org/10.1680/jgeot.15.P.115.

Zhou, H., Kong, G.Q., Liu, H.L. and Laloui, L. (2018), "Similarity solution for cavity expansion in thermoplastic soil", *Int. J. Numer. Anal. Met.*, **42**(2), 274-294. https://doi.org/10.1002/nag.2724.

Zhou, H., Liu, H.L., Zha, Y.H. and Feng, Y. (2017), "A general semi-analytical solution for consolidation around an expanded cylindrical and spherical cavity in modified cam clay", *Comput. Geotech.*, **91**, 71-81. https://doi.org/10.1016/j.compgeo.2017.07.005.

Zou, J.F. and Xia, M.Y. (2017), "A new approach for the cylindrical cavity expansion problem incorporating deformation dependent of intermediate principal stress", *Geomech. Eng.*, **12**(3), 347-360. https://doi.org/10.12989/gae.2017.12.3.347.

Zou, J.F. and Zuo, S.Q. (2017), "Similarity solution for the synchronous grouting of shield tunnel under the vertical non-axisymmetric displacement boundary condition", *Adv. Appl. Math. Mech.*, **9**(1), 205-232. https://doi.org/10.4208/aamm.2016.m1479.

Zou, J.F., Yang, T., Ling, W., Guo, W.J. and Huang, F.L. (2019), "A numerical stepwise approach for cavity expansion problem in strain-softening rock or soil mass", *Geomech. Eng.*, **18**(3), 225-234. http://doi.org/10.12989/gae.2019.18.3.225.

JS